INT. J. REMOTE SENSING, 2003, VOL. 24, NO. 9, 1949–1956

Taylor & Francis
Taylor & Francis Group

Technical note

Classification of off-diagonal points in a co-occurrence matrix

D. B. HANN,

Department of Mechanical Engineering, King's College London, University of London, Strand, London, WC2R 2LS, UK; e-mail: david.hann@kcl.ac.uk

A. M. S. SMITH*

Department of Geography, King's College London, University of London, Strand, London, WC2R 2LS, UK; e-mail: alistair.smith.kcl@kcl.ac.uk

and A. K. POWELL

Department of Physics, King's College London, University of London, Strand, London, WC2R 2LS, UK; e-mail: kp@maxwell.ph.kcl.ac.uk

(*Received 26 November 2001; in final form 15 March 2002*)

Abstract. The classification of the off-diagonal points within a typical grey level co-occurrence matrix (GLCM) is discussed through the application of an intuitive nearest peak and a boundary rule method. Both approaches are applied to a synthetic image consisting of five regions with varying amounts of added random noise and also to an image containing three Brodatz textures of different standard deviation. The two approaches correctly identify the majority of the internal region pixels. However, the nearest peak method is shown to produce serious misclassifications at the region boundaries in the form of bands of additional regions. The boundary rule method does not show this characteristic. The overall classification accuracy and the k_{hat} statistic were used to test the performance of each technique.

1. Introduction

The determination of image features is a subject undergoing much research in the analysis of Earth observation imagery. One technique that has recently been receiving increasing attention in the remote sensing community is the use of co-occurrence matrices for the identification of textural classes within an image (Carlson and Ebel 1995, Karathanassi *et al.* 2000, Kiema 2002, Smith *et al.* in press).

Classification techniques based on co-occurrence matrices use either the inherent textural properties of image entropy, homogeneity, dissimilarity, contrast, etc., (Haralick and Shanmugam 1974, Franklin *et al.* 2001, Kiema 2002) or work by

*Corresponding author.

International Journal of Remote Sensing
ISSN 0143-1161 print/ISSN 1366-5901 online © 2003 Taylor & Francis Ltd
http://www.tandf.co.uk/journals
DOI: 10.1080/01431160210154074

mapping the co-occurrence incidence information in the matrix to specific image textures (Paplinski and Boyce 1997, Karathanassi *et al.* 2000, Smith *et al.* in press).

Whilst image classification techniques using grey level co-occurrence matrices (GLCMs) have been useful in the determination of regions, the edges of the resultant segmentations have always been poorly defined. In most textural classification techniques the region boundaries frequently produce misclassification from operators convolved with irregular edges. However, in the case of a GLCM-based technique, another potential source of error arises from incorrect classification of the off-diagonal points. In the GLCM the regions are easily identified from the dominant peaks on the centre diagonal whilst the boundary information is contained in the off diagonal points. These off-diagonal boundary pixels need to be associated with the correct regions in order to produce an accurate classification, but this has proved difficult (Paplinski and Boyce 1997).

To avoid this risk of boundary-pixel misclassification, previous researchers have masked all near-boundary pixels to zero. This can be done either by defining all image pixels within a set distance of a boundary as belonging to a default class of zero (Karathanassi *et al.* 2000), or by setting all the pixels in the GLCM that lie a set distance away from the centre diagonal to a default class (Paplinski and Boyce 1997). Once the majority of boundary pixels in the GLCM are removed the textural data can be classified by projecting the pixels onto the nearest peak on the centre diagonal (Paplinski and Boyce 1997). This approach, although intuitive, is not the most accurate classification method as the majority of the points in the GLCM can in fact be assigned to the correct region by the application of a simple boundary rule, which this paper will describe.

This technical note will demonstrate an improved approach by which the off-diagonal boundary pixels can be classified since it has been observed that previous off-diagonal classification methods are not well defined in the literature. The method applied is a simple boundary rule for an operator applied in one direction and is demonstrated on a synthetically generated noisy image as well as on a set of Brodatz textures (Brodatz 1966). The Brodatz textures were chosen as they are natural textures and should thus suggest the effects of the different methods on remotely sensed data. The textures from the Brodatz album are widely used in region classification literature (Unser 1995, Hsin 2000).

The performance of each technique applied will be determined through the use of the overall accuracy and the k_{hat} statistic as these measures each indicate different measures of accuracy (Karathanassi *et al.* 2000).

2. Background

Traditionally GLCMs were defined by plotting the incidences of (x, y) pixel intensity pairs on to a matrix (Haralick *et al.* 1974). However, in recent years, researchers in medical imaging and other imagery fields have expanded this concept to adjacent regions or groups of pixels (Paplinski and Boyce 1997, Barman *et al.* 2000, Smith *et al.* in press). Detailed descriptions of the properties of single pixel pairs and pixel groups can be found in the extensive literature (Haralick *et al.* 1974, Paplinski and Boyce 1997, Karathanassi *et al.* 2000, Kiema 2002).

3. Test data

3.1. *Synthetic image*

This image is shown in figure 1(*a*) and contains five regions of both varying intensity and degree of added random noise. Plotting the values obtained through

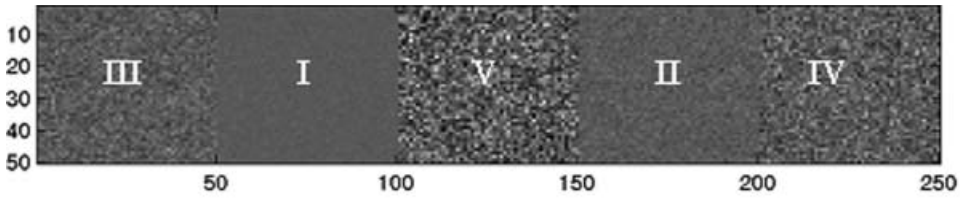

(*a*)

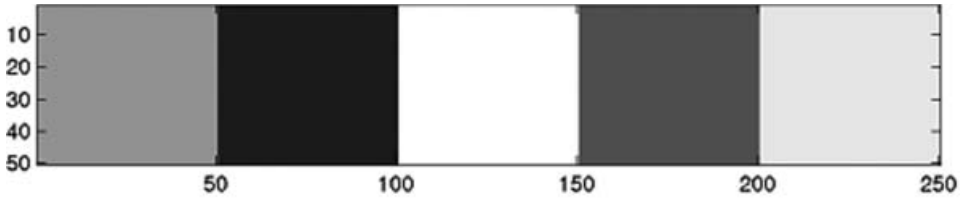

(*b*)

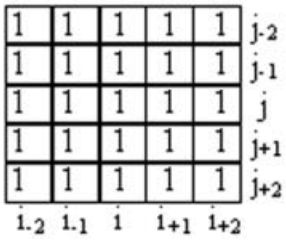

(*c*)

Figure 1. (*a*) Systematic image containing five regions with infrared standard deviation. Adding different degrees of random noise to each region forms the synthetic image. The roman numerals relate to the region class in terms of its position on the co-occurrence matrix in figure 3. (*b*) The expected class image depicts the 'perfect' classification. (*c*) A standard deviation operator of size $n=3$.

the convolution of this image with the operator, as shown in figure 1(*c*), in the horizontal direction produces the co-occurrence matrix shown in figure 3(*a*).

3.2. *Brodatz textures*

This image consists of three different Brodatz textures and is shown in figure 2(*a*) and the resulting matrix is depicted in figure 4(*a*). The three textures were chosen due to their similar texture type.

3.3. *Spatial operators*

The (x, y) values are obtained by using the unity square standard deviation operators:

$$x = \mathrm{STDEV}(i_{-(n-1)}, \ldots i_{-2}, i_{-1}, i; j_{-(n-1)}, \ldots j, \ldots j_{+(n-1)}) \quad (1)$$

$$y = \mathrm{STDEV}(i, i_{+1}, i_{+2}, \ldots i_{+(n-1)}; j_{-(n-1)}, \ldots j, \ldots j_{+(n-1)}) \quad (2)$$

An example combined spatial operator, of size $n=3$, is shown in figure 1(*c*). In the analysis of GLCM, previous researchers have noted that the operator size influences the performance of the classification techniques as factors such as the spatial size of

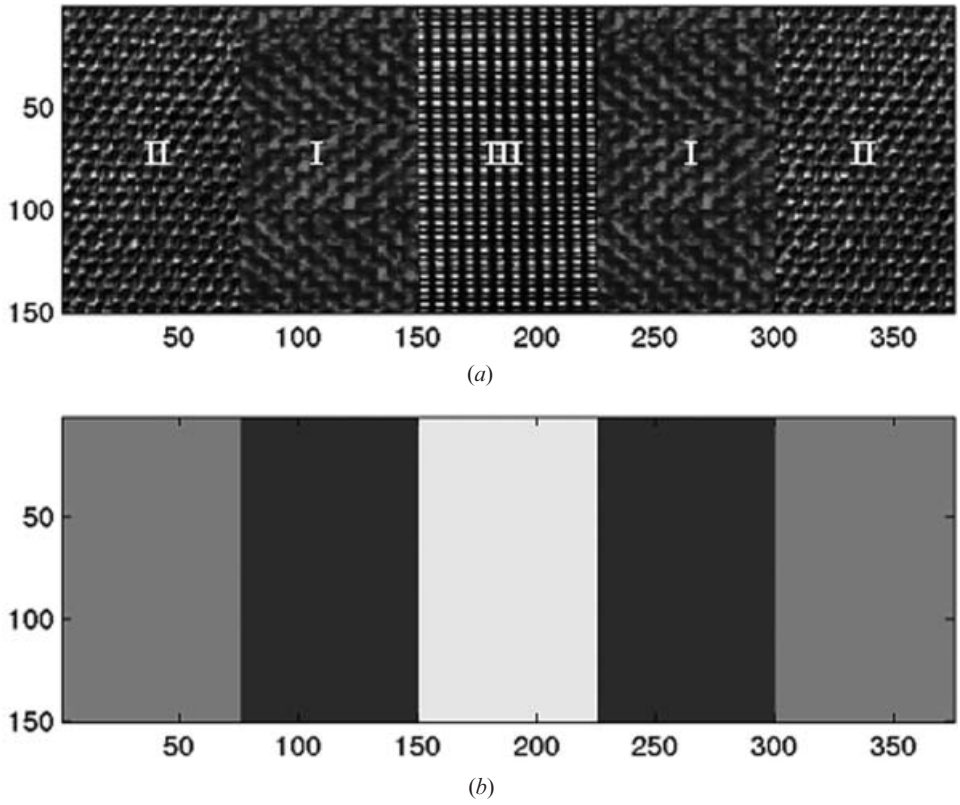

Figure 2. (*a*) Five regions representing three Brodatz textures, each Brodatz texture having a different standard deviation. (*b*) Classification map of the Brodatz image depicting the 'perfect' classification.

the textures and regions become more important at differing spatial scales (Karathanassi *et al.* 2000). The operator size, in terms of n, chosen for the synthetic and Brodatz images were 11 and 21 respectively.

4. Methodology

The operator defined by equations (1) and (2) moves across each image in the horizontal direction. For each horizontal pass on figure 1(*a*) the general location of each (x, y) incidence pair on the GLCM follows the black arrows that are marked on the matrix in figure 3(*a*).

In the GLCM in figure 3(*a*) it is seen that, whilst the operator remains within region III of figure 1(*a*), the location of the (x, y) values remains near the centre diagonal near location III. However as the operator approaches the boundary with region I of figure 1(*a*), the (x, y) incidence points in figure 3(*a*) move left in the horizontal direction (with constant y) before flipping at C to the vertical (with constant x) and moving upwards to location I near the centre diagonal. At location I the operator is now completely within region I of figure 1(*a*), and the points will only move away towards A when the operator approaches the region V boundary. The correct classification procedure of the off-diagonal points should match these

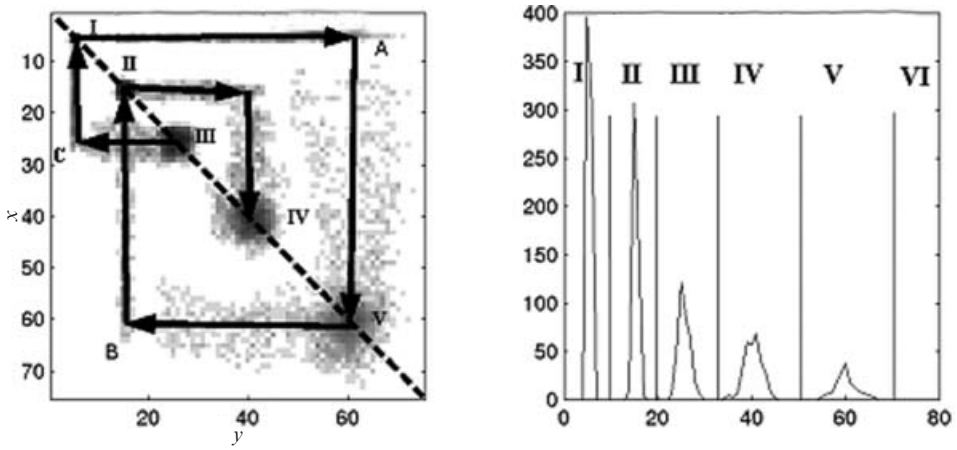

(*a*) (*b*)

Figure 3. (*a*) The GLCM showing position of region pixels obtained by applying the operator in the horizontal direction to the synthetic image in figure 1. The black arrows show the order that points are placed onto the GLCM in each horizontal pass. The horizontal and vertical features from the near boundary pixels are easily apparent. (*b*) Diagonal GLCM showing position of region peaks. The projection of the centre diagonal shows the identified regions that are used in the classification process.

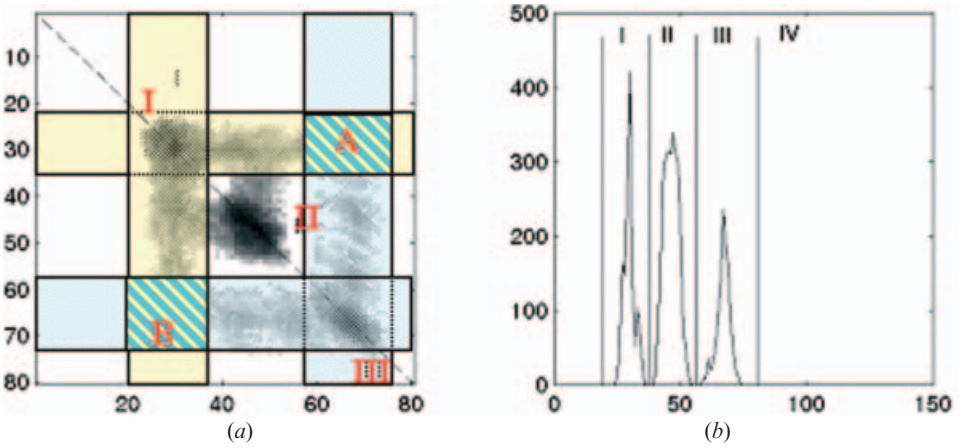

(*a*) (*b*)

Figure 4. (*a*) The log of the GLCM showing regions for the Brodatz texture set image highlights the boundary features. The semi-transparent slices show the pixels that could be classed as belonging to region I (yellow) or region II (blue). The areas marked by A or B could belong to either region and so the boundary rule must be applied. (*b*) Diagonal of GLCM showing regions. As the regions in figure 2 are more similar than those in figure 1, the region peaks are much more compacted. This increases the risk of boundary misclassification.

off diagonal points to one of the corresponding (x, y) values on the centre diagonal. The main problem is therefore to make sure that the correct x or y value is taken.

The corrected technique can be simplified into three steps and will be demonstrated using the GLCM in figure 4(*a*), produced from applying the operator to the Brodatz texture test image (figure 2(*a*)).

1. Regions are identified on the diagonal of the co-occurrence matrix. These regions, as shown in figure 4(*b*), do not overlap and each region is defined by taking the midpoints between adjacent peaks.
2. The regions are projected horizontally and vertically, shown as semi-transparent blocks in figure 4(*a*), to cover whether the operator is approaching from the left or right. Any off-diagonal point is therefore at the crossover of two of these region blocks [A and B in figure 4(*a*)]. The point is then known to be associated to one of these two regions and thus has two region values. Therefore point A in figure 4(*a*) could be in region I or region III, so its region value $(X_i, Y_i) = (\mathrm{I}, \mathrm{III})$.
3. By comparing these region values with those adjacent to the region, a rule is produced that will ensure that the correct region designation is taken. In this case we took the x region unless the previous region to the left was different, where upon we took the y region as the correct value. The rule is summarized by:

$$\text{If } xi \neq yi-1 \text{ then region} = Yi \text{ else region} = Xi \tag{3}$$

Figure 4(*a*) also demonstrates why the closest peak technique gives incorrect classifications at the edges. In this case, at sites A and B the nearest peak approach classifies all the pixels within these overlapping sections to region II. This creates an additional erroneous band on the classification. The number of additional regions is equal to the number of possible regions that lie between the two that the operator is crossing. In the extreme, in figure 1(*b*) the operator moves from region I to region V and produces three additional regions in figure 5(*b*). Thus, if the image contained many regions and if there was a large contrast between them, the closest peak method would produce a high percentage of edge pixel misclassification.

It must be emphasized that the boundary rule does not produce perfect classifications at the boundaries and factors such as operator size, boundary thickness and contrast between regions will still affect the accuracy. The classifications do not, however, produce fictitious regions at the class boundaries, which is important for remote sensing applications.

5. Results and discussion

By applying both techniques to figures 1(*a*) and 2(*a*) the classified datasets were produced. The classifications produced by using the nearest peak approach are shown in figures 5(*b*) and 6(*b*) and, as predicted, produce serious misclassifications at the region boundaries. The overall accuracy for each classification was calculated to be 81.43% and 88.07% with $\kappa = 0.7676$ and 0.8119 respectively. These results are similar to results for co-occurrence matrix classification performances in the literature (Laine and Fan 1993, Karathanassi *et al.* 2000).

The boundary rule technique produced the classified images shown in figures 5(*a*) and 6(*a*). Overall accuracy values of 96.93% and 93.93% were obtained with k_{hat} values of 0.9616 and 0.9056 obtained respectively.

6. Conclusions

We have demonstrated that by relating the off-diagonal points to the horizontal and vertical extensions of the regions on the centre diagonal, significant increases in overall classification accuracy can be obtained. The magnitude of the accuracy improvement will depend on a number of factors within the image, for example the

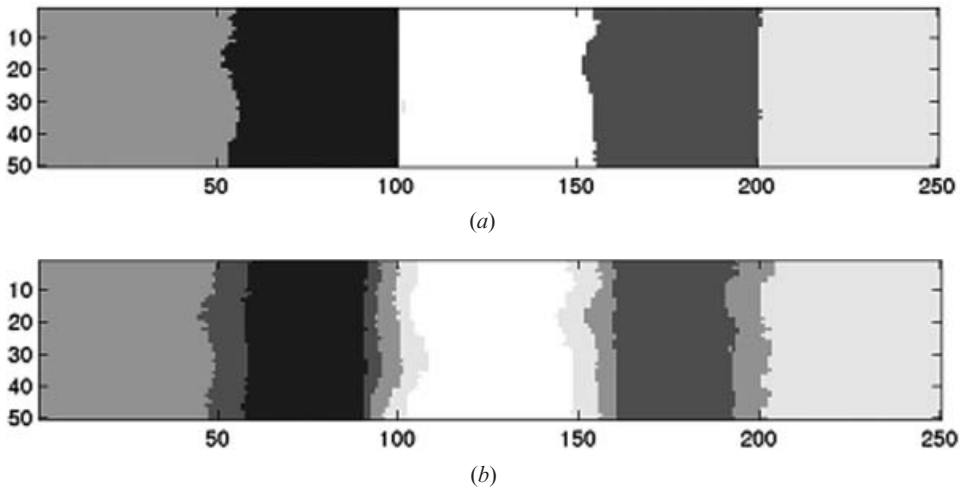

Figure 5. Segmented image using (*a*) boundary rule (accuracy = 96.93, $\kappa = 0.9616$) and (*b*) closest peak (accuracy = 81.41, $\kappa = 0.7676$) classification of the synthetic image in figure 1. The nearest peak approach has produced bands of additional regions at the boundaries.

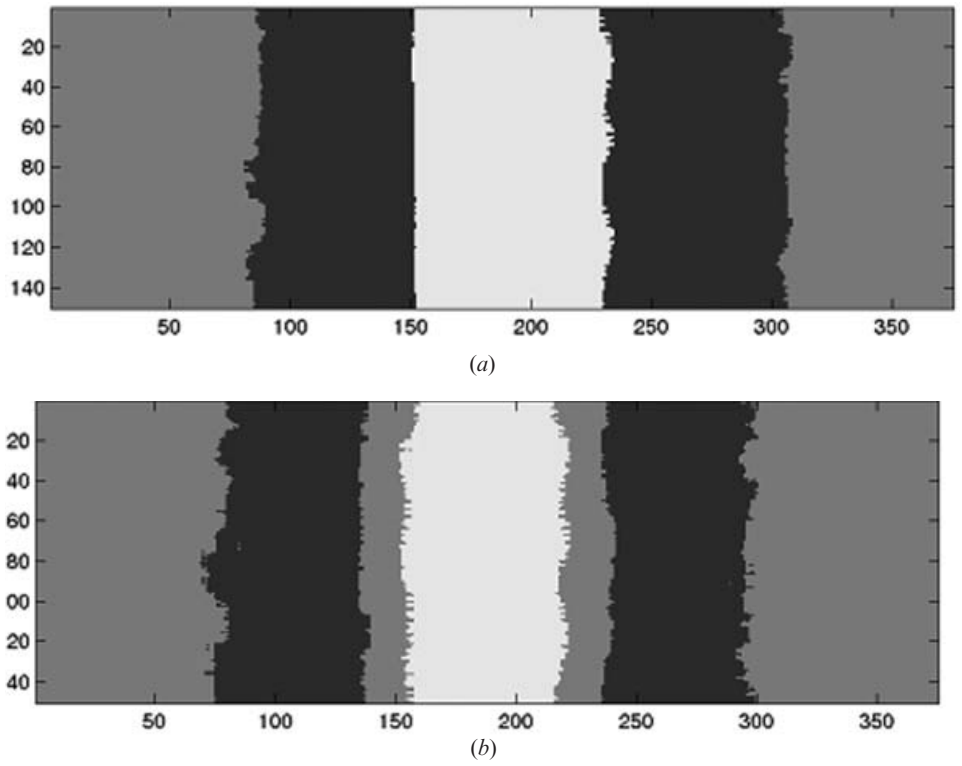

Figure 6. Segmented image using (*a*) boundary rule (accuracy = 93.93, $\kappa = 0.9056$) and (*b*) closest peak (accuracy = 88.07, $\kappa = 0.8119$) classification of the set of Brodatz textures in figure 2.

size of the regions, the relative contrast between adjacent regions and the total number of regions. However, in all cases we expect this boundary rule method to outperform the previously applied closest peak approach, as we have found during analysis of simulated imagery.

Acknowledgments

A. M. S. Smith is supported by the NERC/GANE Thematic Programme studentship (NER/S/R/2000/04057).

References

Barman, S. A., Hollick, E. J., Boyce, J. F., Spalton, D. J., Uyannonyara, B., Meacock, W. R., and Sanguinetti, G., 2000, Quantification of posterior capsule opacification in digital retroillumination images using a computational method based on texture analysis. *Investigative Ophthalmology and Visual Science*, **41**, 3882–3892.

Brodatz, P., 1966, *Textures: A photographic album for artists and designers*. New York: Dover, 265.

Carlson, G. E., and Ebel, W. J., 1995, Technical Note: Co-occurrence matrices for small region texture measurement and comparison. *International Journal of Remote Sensing*, **16**, 1417–1423.

Franklin, S. E., Wulder, M. A., and Gerylo, G. O., 2001, Texture analysis of IKONOS panchromatic data for Douglas-fir forest age class separability in British Columbia. *International Journal of Remote Sensing*, **22**, 2627–2632.

Haralick, R. M., and Shanmugam, K., 1974, Combined spectral and spatial processing of ERTS imagery data. *Journal of Remote Sensing of Environment*, **3**, 3–13.

Haralick, R. M., Shanmugam, K., and Dinstein, I., 1974, Textural features for image classification. *IEEE Transactions on Geosciences and Remote Sensing*, **SMC-3**, 610–621.

Hsin, H., 2000, Texture segmentation using modulated wavelet transform. *IEEE Transactions on Image Processing*, **9**, 1299–1302.

Karathanassi, V., Iossifidis, C. H., and Rokos, D., 2000, A texture-based classification method for classifying built areas according to their density. *International Journal of Remote Sensing*, **21**, 1807–1823.

Kiema, J. B. K., 2002, Texture analysis and data fusion in the extraction of topographic objects from satellite imagery. *International Journal of Remote Sensing*, **23**, 767–776.

Laine, A., and Fan, J., 1993, Texture classification by wavelet packet signatures. *IEEE Transactions on Pattern Analysis and Machine Intelligence*, **15**, 1186–1191.

Paplinski, A. P., and Boyce, J. F., 1997, Segmentation of a class of ophthalmological images using a directional variance operator and co-occurrence arrays. *Optical Engineering*, **36**, 3140–3147.

Smith, A. M. S., Wooster, M. J., Powell, A. K., and Usher, D., in press, Texture based feature extraction: application to burn scar detection in Earth Observation satellite imagery. *International Journal of Remote Sensing*, **23**, 1733–1739.

Unser, M., 1995, Texture classification and segmentation using wavelet frames. *IEEE Transactions on Image Processing*, **4**, 1549–1560.